PERMEAMETRY
IN THE
KNUDSEN-FLOW REGIME

A THESIS

Presented to

The Faculty of the Division of Graduate

Studies and Research

By

John F. Brock

In Partial Fulfillment

of the Requirements for the Degree

Master of Science in Chemical Engineering

Georgia Institute of Technology

December, 1971

PERMEAMETRY

IN THE

KNUDSEN-FLOW REGIME

Approved:

[redacted]

Chairman

[redacted]

[redacted]

Date approved by Chairman: 11-22-71

In presenting the dissertation as a partial fulfillment of the requirements for an advanced degree from the Georgia Institute of Technology, I agree that the Library of the Institute shall make it available for inspection and circulation in accordance with its regulations governing materials of this type. I agree that permission to copy from, or to publish from, this dissertation may be granted by the professor under whose direction it was written, or, in his absence, by the Dean of the Graduate Division when such copying or publication is solely for scholarly purposes and does not involve potential financial gain. It is understood that any copying from, or publication of, this dissertation which involves potential financial gain will not be allowed without written permission.

7/25/68

ACKNOWLEDGEMENTS

The author wishes to express his appreciation to his thesis advisor, Dr. Clyde Orr, Jr., for proposing the problem and for his many helpful suggestions. He is also grateful to Dr. C. A. Gorton and Dr. M. J. Matteson for reviewing this work.

The author particularly wishes to express his thanks to his wife, Mary R. Brock, for her endless understanding and for her cheerful assistance in the typing of this thesis.

TABLE OF CONTENTS

LIST OF TABLES

LIST OF ILLUSTRATIONS

SUMMARY

The determination of surface areas of finely divided materials by Knudsen-flow permeametry involves the measurement of resistance to flow of a gas through a powder bed at low pressures. Permeametry as a means of measuring surface area was first suggested in 1937, and has since undergone many refinements. Various permeability equations have been derived, but the one that is of primary concern in this investigation is the equation for Knudsen flow derived by assuming 100 per cent specular reflection of gas molecules. This equation has been used to determine values of specific surface area for non-porous materials that were in agreement with low temperature gas adsorption areas, the present standard for total area evaluation.

The purpose of this study was to (1) make significant mechanical improvements in available permeametric equipment; (2) re-examine the proposition that permeametric surface areas determined by the Knudsen-flow equation are equal to gas adsorption areas for non-porous powders; and (3) determine if, in the case of porous powders, the external surface area determined by permeametry could be combined with the internal pore area determined by mercury penetration porosimetry to give the total surface area as determined by gas adsorption.

For experimentation purposes, 16 materials were selected having total specific surface areas ranging from 0.15 to 70.0 m^2/gram. Seven of the samples were essentially non-porous; the remaining nine were either moderately porous or highly porous. The permeametric surface areas determined for the seven non-porous powders differed from the gas adsorption areas by a minimum of 2.8 and a maximum of 13.3 per cent. This agreement suggests that for non-porous materials, Knudsen-flow permeametry areas are indeed equal to gas adsorption areas within the reliability of both measurements.

The combined areas for the porous powder samples, determined by adding the permeametry areas and the porosimetry areas, differed from corresponding gas adsorption areas by a minimum of 0.0 and a maximum of 28.3 per cent. This agreement suggests that the total surface area of most porous powders may reasonably be obtained by combining the permeametry and the porosimetry areas and that Knudsen-flow permeametry indicates surface areas exclusive of pores, i.e., the external area. It is recommended that further investigation be undertaken to ascertain that this technique of adding areas is permissible for all types of powders.

CHAPTER I

INTRODUCTION

The permeametry method of measuring specific surface areas of powders is a well-known technique (1,2,3,4,5,6). Basically, a permeameter consists of a sample holder for confining the powder to be measured, a pump for moving a gas such as air or helium through the powder bed, and gauges to measure the gas flow rate and the pressure drop across the powder. From these data, the specific surface area of the powder may be calculated. Since the permeameter itself is relatively simple and since the necessary measurements may be made rapidly, permeametry is an attractive method of determining specific surface area. However, in the development of permeametric theory, various assumptions are made. Therefore, permeametry surface areas must always be interpreted with these assumptions in mind.

Permeametry as a method of specific surface measurement was first proposed by Carman (7,8) using the assumption that flow through a powder bed could be approximated by considering it as flow through a bundle of capillary tubes in a parallel array. Obviously, the surface area that is determined using the capillary analogy is the external surface area only. Any internal surface due to pores is neglected, because such pores do not contribute to

flow. The equation that was developed, called the Kozeny-Carman equation* is:

$$S_w = \frac{1}{\rho}\left[\frac{A\,\Delta P}{K_1 L Q \eta RT}\,\frac{\epsilon^3}{(1-\epsilon)^2}\right]^{\frac{1}{2}} \qquad (1)$$

Carman's early work in permeametry was accomplished using liquids instead of gases as the fluid. Later, however, Carman and other workers in the field discovered that the surface areas of powders with large areas could not be determined using a liquid, but could be approximated for coarse powders if a gas, such as air, was employed (9,10).

In 1947, Rigden and Arnell (11,12) showed that the Kozeny-Carman equation must be modified to take into account the effect of "slip" at the walls of the pores in the bed of powder. The permeability equation that resulted was used in various forms by a number of authors (13,14) to measure the specific surface areas of powders. All forms of this equation have been shown to reduce to (15):

$$\frac{QL}{\Delta PA} = \frac{\epsilon^3 \bar{p}}{K_1 (1-\epsilon)^2 S_w^2 \rho^2 \eta RT} + \frac{K_2 \epsilon^2}{(1-\epsilon) S_w \rho (2\pi MRT)^{\frac{1}{2}}} \qquad (2)$$

The first term, the Kozeny-Carman term, gives the contribution due to viscous flow, while the second term gives the contribution due to Knudsen, or molecular, flow.

*See Nomenclature, Appendix A, page 28.

The Kozeny-Carman term describes the flow of a gas through a bed of particles greater than 10μ in diameter at atmospheric pressure. This condition, called viscous flow, occurs when the mean free path of the gas molecules is considerably less than the diameter of the void spaces.

If the particles are coarse and the pressure is greatly reduced or if the particles are fine and the pressure is near atmospheric, the mean free path of the gas molecules is approximately equal to the diameter of the channel. In this flow condition, the gas molecules "slip" at the boundaries, and the flow is defined by some combination of the above two terms.

If the gas pressure is reduced until the mean free path of the gas molecules is greater than the channel diameter by a factor of 10, the flow condition is termed Knudsen flow (16) and is described by the second right-hand term of Equation 2.

In applications of permeametry, both purely viscous flow and purely Knudsen flow are employed; however, this investigation is concerned with Knudsen-flow permeametry only. The equation that is now of interest involves only the second term of Equation 2. The describing equation may be written:

$$\frac{QL}{\Delta PA} = \frac{K_2 \epsilon^2 \pi}{(1-\epsilon) S_w \rho (2\pi MRT)^{\frac{1}{2}}} \qquad (3)$$

Knudsen-flow permeametry has been investigated by several workers (13,17,18), each of whom employed different assumptions to arrive at an equation like Equation 3 with directly measurable quantities. These equations vary, for the most part, only in the value assigned to K_2.

The most reasonable of the various equations (19) is developed by assuming 100 per cent specular reflection, i.e., all the gas molecules are specularly reflected from the powder surface. Helium is essentially non-adsorbing at room temperature and, hence, should give nearly 100 per cent specular reflection. This assumption gives K_2 in Equation 3 a value of $48/13\pi$. Equation 3 then becomes:

$$S_w = \frac{24}{13}\sqrt{\frac{2}{\pi}} \frac{\epsilon^2 A \Delta P}{(1-\epsilon)\rho L Q (MRT)^{\frac{1}{2}}} \qquad (4)$$

Equation 4 has been employed with helium as the flowing gas (3) to obtain specific surface area results that are quite close to nitrogen adsorption areas for powders without, or with few, internal pores.

The general purpose of this investigation was to (1) make significant improvements in the available permeametric equipment; (2) ascertain that permeametric surface areas determined by using Equation 4 are consistent with gas adsorption areas if the powders are non-porous; and (3) determine if, in the case of porous powders, the external surface area as determined by a Knudsen-flow permeameter

could be added to the internal pore area as measured by mercury penetration (20) to give a value approximately equal to the total surface area as determined by low temperature gas adsorption.

CHAPTER II

INSTRUMENTATION AND EQUIPMENT

Alteration to Existing Permeameter

The permeametric equipment that was available for this study was a Knudsen-flow Permeameter, Model 1401, built by Micromeritics Instrument Corporation, Norcross, Georgia. Before this instrument was employed, however, several significant changes were made. These alterations may be understood more clearly by referring to Figure 1, a diagram of the Model 1401 Permeameter, and to Figure 2, a diagram of the altered instrument. The absolute pressure gauge was replaced by a pressure transducer, Model P/N 41GB, Consolidated Controls Corporation, and a Weston Ammeter, 0 to 200 microamperes. The ammeter-pressure transducer system had a faster response than the pressure gauge, primarily because the system volume was considerably reduced. Also, the transducer-ammeter system removed the problems of "drifting" at a given setting of the micrometer valve.

The second significant alteration was the replacement of the flexible bellows in the Model 1401 with a larger, temperature-controlled bellows. Temperature control was installed to eliminate expansion and contraction effects associated with the bellows and its housing because of ambient temperature changes. By increasing the size,

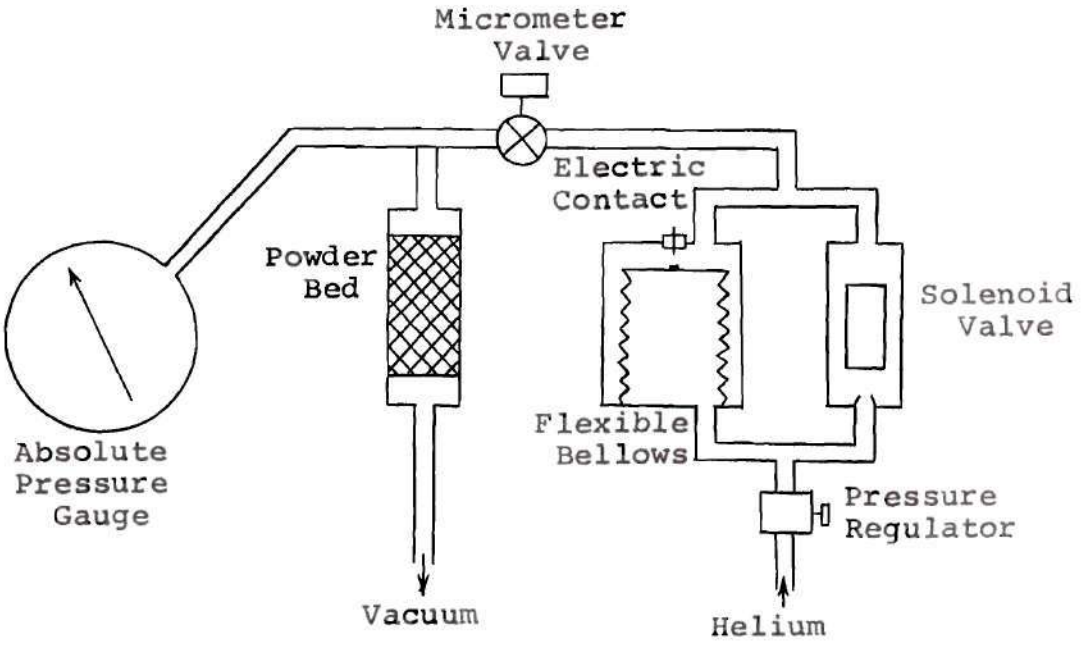

Figure 1. Diagram of Model 1401 Permeameter.

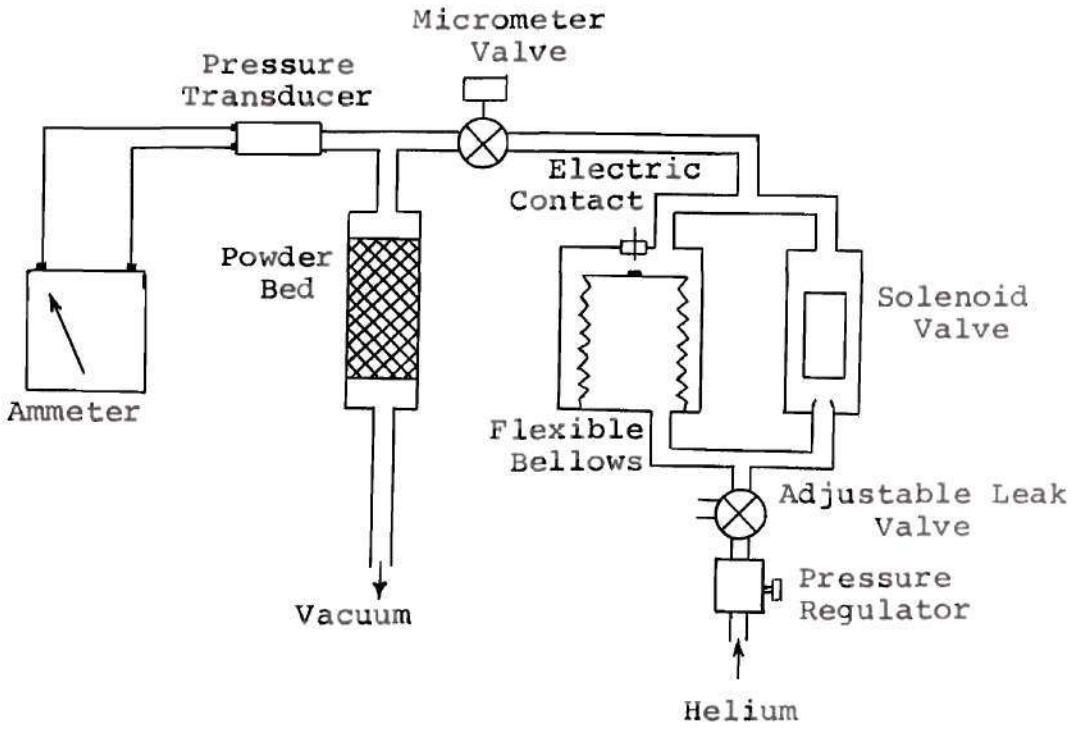

Figure 2. Diagram of Altered Permeameter.

the sensitivity and flexibility of the bellows system were increased greatly. In fact, the first design for the system was so sensitive that vibrations from another machine in the laboratory or from a truck passing outside caused the bellows to vibrate irregularly. To eliminate these vibration problems, the bellows was mounted on a foam-rubber pad; a conducting plate was attached to the bellows so as to move through the poles of a permanent magnet to dampen all rapid, i.e., vibratory, motion; and all rigid connections to the bellows were replaced by flexible vacuum hose. These alterations eliminated vibration problems.

The third change to the Model 1401 was the installation of an adjustable leak valve immediately downstream from the pressure regulator. This valve permitted an extremely small flow from the system, so that when the micrometer valve was adjusted, the pressure in the gas-feeding portion did not change erratically, but rather, adjusted to the desired pressure of 1000 mm Hg quickly.

Description of Equipment

The altered permeameter consists of a 0 to 200 microampere ammeter, a pressure transducer, a micrometer flow-regulating valve, a solenoid valve, a temperature-controlled flexible bellows, a timer, a pressure regulator, an adjustable leak valve, a powder holder, a vacuum pump, and a cylinder of helium. The powder holder is a metal cylinder with a porous bottom of sintered metal. The bottom of the

holder is covered with a piece of filter paper during a test to prevent clogging of the porous plate. The bed is formed by compressing a weighed quantity of powder into the holder.

The pressure transducer detects the pressure drop across the powder bed and converts this pressure into microamperes. The design of the circuit* is such that the indicated current in microamperes divided by a factor of ten gives the pressure in millimeters of mercury. The helium is maintained at a constant pressure of 1000 mm Hg by the pressure regulator and is fed into the bed through a solenoid valve and bellows system. A vacuum pump removes the helium on the downstream side of the powder bed. The solenoid valve is normally open. When the timer is started, the solenoid valve is closed and the gas outside the bellows is fed to the powder. The bellows expands and makes electrical contact which stops the timer, opens the solenoid valve, and allows the bellows to reset itself. The desired quantity of helium is passed through the bed by adjusting the contact point. Thus, the timer actually measures gas flow rate.

The gas-feeding portion of the equipment is separated from the powder bed and pressure transducer by a micrometer needle valve. This valve restricts the gas flow and thus permits adjustment of the pressure and flow rate.

*Built especially for this study by Mr. Ronnie Camp of the Micromeritics Instrument Corporation, Norcross, Georgia.

The adjustable leak valve introduces a very small leak in the system which prevents the pressure in the gas feeding portion from changing significantly when the micrometer valve is adjusted.

All components of the permeameter are connected with 1/4 inch stainless steel tubing except for connections to the bellows system which are 1/4 inch vacuum hose as described above.

A description of the powder samples employed appears in Table 1. All densities and total surface areas were determined and furnished by the suppliers.

Mercury Penetration Porosimeter data were supplied by Micromeritics Instrument Corporation for all polyvinyl chloride and iron oxide samples. Porosimeter data for boron nitride and cupric carbonate samples were determined by the author using a Micromeritics Instrument Corporation, Model 900 Series, Mercury Penetration Porosimeter.

Table 1. Description of Powder Samples

Sample	Density (g/cm^3)	Total Specific Surface Area (m^2/g)	Data Source
Iron Blue	1.70	70.0[a]	Mic.Inst.Corp.
Titanium Dioxide	4.17	54.1[a]	Mic.Inst.Corp.
Tungsten	19.3	0.52[b]	Mic.Inst.Corp.
Polyvinyl Chloride	1.52	1.28[b]	Mic.Inst.Corp.
Polyvinyl Chloride	1.57	1.27[b]	Mic.Inst.Corp.
Polyvinyl Chloride	1.60	1.10[b]	Mic.Inst.Corp.
Polyvinyl Chloride	1.52	0.15[b]	Mic.Inst.Corp.
Cupric Carbonate-A	3.95	26.8[a]	Mic.Inst.Corp.
Cupric Carbonate-B	3.95	19.1[a]	Mic.Inst.Corp.
Iron Oxide-A	5.25	5.70[a]	Mic.Inst.Corp.
Iron Oxide-B	5.25	9.50[a]	Mic.Inst.Corp.
Iron Oxide-C	5.25	5.62[a]	Mic.Inst.Corp.
Boron Nitride-A	2.25	18.4[a]	Dr.R.A.Pierotti Georgia Tech
Boron Nitride-B	2.25	4.98[a]	Dr.R.A.Pierotti Georgia Tech
Carbon Black-A	1.87	14.4[c]	Dr.B.W.Davis Georgia Tech
Carbon Black-B	1.89	7.5[c]	Dr.B.W.Davis Georgia Tech

a-N_2 adsorption surface area determination using B.E.T. method.
b-Kr adsorption surface area determination using B.E.T. method.
c-Surface area determined by electron microscopy.

CHAPTER III

PROCEDURE

Preparation of the Packed Bed

All powders were thoroughly dried before packing. A disk of filter paper 3/4 inches in diameter was placed upon the sintered metal piece forming the bottom of the sample holder. The cylinder forming the walls of the powder holder was then pressed against the paper and the retaining nut tightened. The sample was added incrementally, with a plunger being employed to compress the powder after each addition.

The weight of powder in the bed was established from the difference in the weight of powder sample before and after the powder for the bed was extracted. The powder holder had a diameter of 1.346 cm which resulted in a cross-sectional area of 1.42 cm^2. The bed length was determined using a set of calipers. The powder holder was attached to the other components of the system through connections provided in the instrument panel.

Making the Tests

The vacuum pump was started and allowed to pump until the ammeter indicated 10 to 20 microamperes (1 to 2 mm Hg). Residual air was removed by opening the micrometer

valve to flush the system with helium. Flushing with helium for 15 minutes at 150 microamperes caused the ammeter to drop rapidly to zero when the valve was closed.

The micrometer valve was then adjusted so that the ammeter indicated about 140 microamperes. Starting the timer caused one cubic centimeter of helium (at ambient temperature and 1000 mm Hg) to pass through the sample. The values indicated on the timer and the ammeter were recorded. The micrometer valve was then adjusted so that the ammeter indicated a lesser pressure, say about 100 microamperes. The timer was re-zeroed and started. When it stopped, the time and current measurements were recorded as before. This entire process was repeated at ammeter readings of about 60 and 30 microamperes.

Testing a Blank

The resistance to flow that was indicated in a test with a powder contained a contribution from the filter paper and the sintered metal support. Therefore, a test with only the sintered support and the filter paper was made as above except that measurements were taken at much smaller intervals of pressure. The data were then plotted as Pressure Drop *versus* Time on logarithmic paper (see Figure 10, Appendix). This curve was then employed to determine the true pressure loss through any sample by subtracting the loss due to the support and filter from the loss with the support, filter and sample at corresponding passage times.

Calibration of the System

The inlet pressure was maintained at 1000 mm Hg by the pressure regulator. A sensitive mercury manometer was attached immediately downstream of the regulator to assure that this pressure was correct. If the pressure were not 1000 mm Hg, the set screw on the regulator was adjusted so that the pressure was maintained at 1000 mm Hg.

The gas flow from the bellows was established by attaching a sensitive soap-bubble flow meter to the upper sample connector. When gas was supplied to the system, activating the timer initiated flow rate measurement. Since one cubic centimeter of gas at 1000 mm Hg and ambient temperature was the desired volume, the volume measured by the flow meter was 1000/P, where P is atmospheric pressure in mm Hg. Atmospheric pressure in the laboratory was usually about 740 mm Hg, so the measured volume was 1000/740 or 1.35 cc. The screw for adjusting this flow was centrally positioned on top of the bellows unit; it was adjusted until the desired flow was obtained.

Calculation of Results

Each individual set of data, when substituted into Equation 4 gave a specific surface area value. Plotting these surface areas against pressure on a log-arithmetic grid and extrapolating to zero pressure established the true, external specific surface area of the powder. A complete sample treatment of the data is presented in Appendix C.

CHAPTER IV

DISCUSSION OF RESULTS

A summary of results is presented in Table 2. In the first column of the table is listed a description of the material being tested. The second column lists the external specific surface area as determined by Knudsen-flow permeametry. In the third column, the internal area determined by mercury penetration porosimetry is tabulated. The combined area, determined by adding corresponding values from columns two and three, is listed in column four. For comparative purposes, the specific surface area determined by low temperature gas adsorption (B.E.T) or from electron microscopy is given in the last column.

The first seven samples listed in Table 2 are non-porous materials, i.e., their internal area as determined by mercury penetration porosimetry is essentially zero. The values for permeametry surface areas of these seven materials are in excellent agreement with the low temperature gas adsorption values. This observation confirms that for non-porous materials, Knudsen-flow permeametry surface areas are equal to gas adsorption areas. Scanning electron micrographs were made of two representative non-porous samples. The titanium dioxide particles in Figure 3 are seen to be very small, almost spherical, and with no pores in

Table 2. Experimental Surface Areas

Description of Material	Permeametry External Area (m^2/g)	Porosimetry Internal Area (m^2/g)	Combined Area (m^2/g)	Gas Adsorption Area (m^2/g)
Iron Blue Pigment	74.1	0	74.1	70.0
Titanium Dioxide	57.0	0	57.0	54.1
Boron Nitride-A	17.2	0	17.2	18.4
Carbon Black-A	14.0	0	14.0	14.4(a)
Carbon Black-B	8.0	0	8.0	7.5(a)
Tungsten	0.48	0	0.48	0.52
Polyvinyl Chloride-A	0.13	0	0.13	0.15
Polyvinyl Chloride-B	0.17	0.94	1.11	1.10
Polyvinyl Chloride-C	0.19	1.12	1.31	1.27
Polyvinyl Chloride-D	0.30	0.75	1.05	1.28
Cupric Carbonate-A	4.2	22.2	26.4	26.8
Cupric Carbonate-B	3.6	15.5	19.1	19.1
Boron Nitride-B	0.27	4.55	4.82	4.98
Iron Oxide-A	1.50	4.48	5.98	5.70
Iron Oxide-B	1.77	8.02	9.79	9.50
Iron Oxide-C	2.10	5.11	7.21	5.62

(a) Determined by electron microscopy.

evidence. The polyvinyl chloride in Figure 4 is also somewhat spherical; its surface is "dimpled" but no pores are apparent.

The remainder of the materials in Table 2 are porous materials, with their pore area ranging from 69.4 per cent for iron oxide-C to 94.5 per cent for boron nitride-B. The values for their combined area listed in column four are generally in agreement with gas adsorption areas listed in column five. Combined area values differ from gas adsorption areas by less than 11 per cent for all samples tested except for iron oxide-B, whose values differ by 28.3 per cent. Thus, this is strong evidence that the true specific surface area of a particulate system can be obtained by combining the external surface area from permeametry with the internal surface area from mercury porosimetry.

Scanning electron micrographs of individual particles from several representative samples were also made in order to confirm results. The boron nitride-B in Figure 5 is seen to consist of very irregular particles having a wide range of sizes and agglomerates of particles. The appearance of numerous pores suggests that the pore area should be much greater than the external area, and this suggestion is borne out by the results in Table 2. Iron oxide-A and iron oxide-C are shown in Figures 6 and 7, respectively. Although the two oxides are obviously not identical, both pictures do show very irregularly shaped particles having

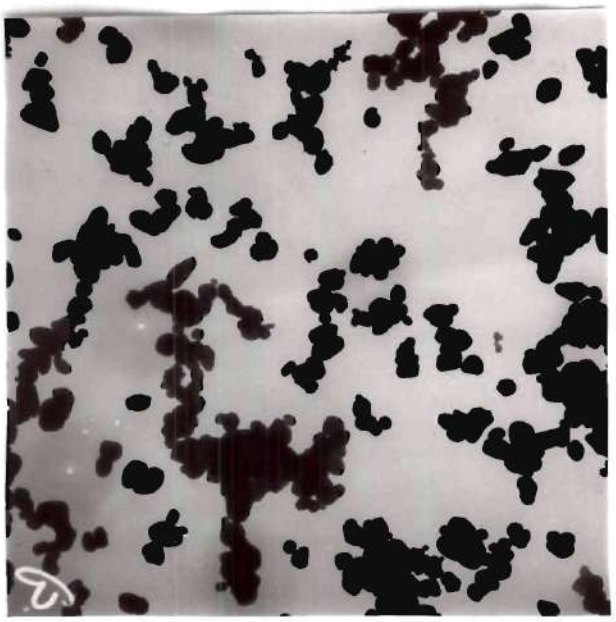

Figure 3. Micrograph of Titanium Dioxide.

1 μ

Figure 4. Micrograph of Polyvinyl Chloride-A.

10 μ

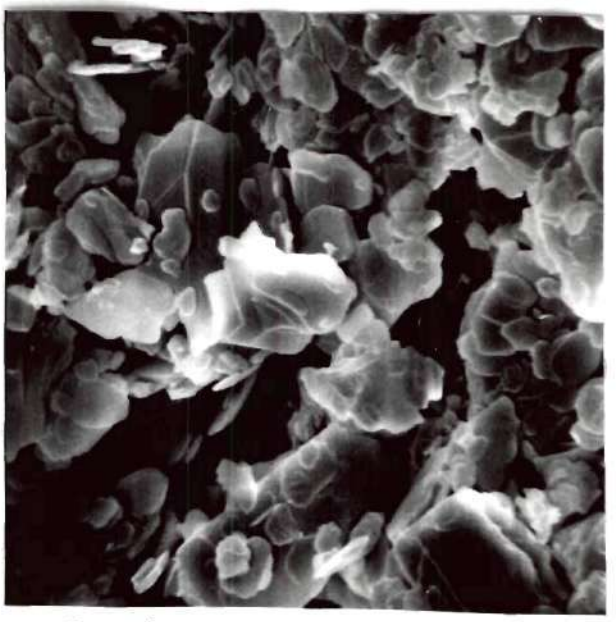

Figure 5. Micrograph of Boron Nitride-B.

10μ

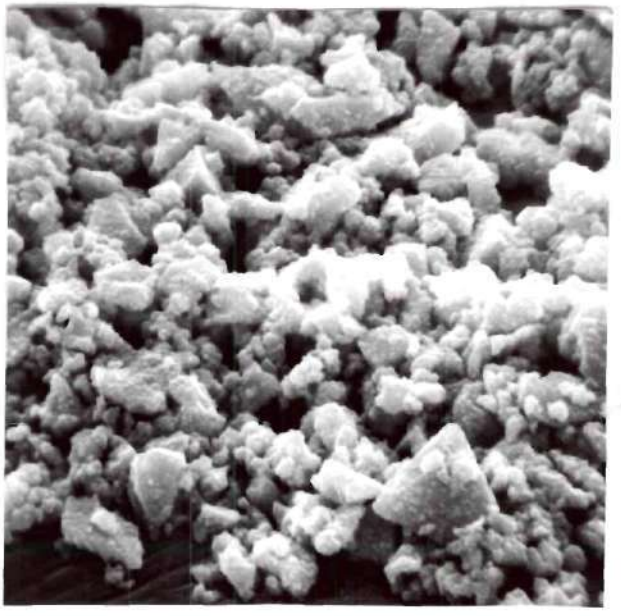

Figure 6. Micrograph of Iron Oxide-A.

10μ

numerous agglomerates and a wide size range. Therefore, the results in Table 2 that show numerous pores are reasonable. Also, the external area of iron oxide-C is somewhat greater than the external area of iron oxide-A, which is expected since the mean particle size of C is slightly less than the mean particle size of A.

A micrograph of polyvinyl chloride-D is shown in Figure 8. This picture actually shows no more pores than does the picture of the non-porous polyvinyl chloride in Figure 4. This is undoubtedly due to the fact that the pictures are not sufficiently magnified to reveal the presence or absence of pores. However, it can be concluded that numerous pores are present in the material of Figure 8 by comparing the sizes of the particles in Figures 4 and 8. If both particulate systems were non-porous, then the system with the smallest mean particle size would have the largest specific surface area. In the case at hand, the PVC-A clearly has the smallest mean particle size, and therefore, should have a larger surface area than PVC-D. However, the gas adsorption area for PVC-A is almost an order of magnitude less than the gas adsorption area for PVC-D. The only possible explanation for this phenomenon is the presence of numerous internal pores in the PVC-D, causing it to have a higher gas adsorption area.

In Figure 9, a micrograph of cupric carbonate-B is shown, and as above, the presence of pores cannot be

Figure 7. Micrograph of Iron Oxide-C.

10 μ

Figure 8. Micrograph of Polyvinyl Chloride-D.

10 μ

Figure 9. Micrograph of Cupric Carbonate-B.

10 μ

established from this picture. However, the presence of pores can be deduced by comparing particle sizes between Figures 4 and 9. Since the cupric carbonate particles are smaller than the PVC-A particles, the external area for cupric carbonate should be the higher of the two. This suggestion holds true, since the external area of cupric carbonate-B was found to be 4.2 m^2/g which is considerably higher than the 0.13 m^2/g for PVC-A. At the same time, it is not at all unreasonable for the cupric carbonate to have a significant internal area, since the particles in Figure 9 are not drastically smaller than the particles in Figure 4.

CHAPTER V

CONCLUSIONS

The following conclusions were drawn from this study:

1. Using Knudsen-flow permeametry and a non-adsorbing gas like helium, Equation 4 gives values for specific surface area that are in good agreement with gas adsorption surface area values when non-porous materials are tested.

2. Equation 4 gives a surface area value that is approximately equal to the external surface area of the material if a porous material is tested.

3. The total surface area of porous powders obtained by summing the external area determined by Knudsen-flow permeametry and the internal area determined by mercury porosimetry differed from the total surface area determined by low temperature gas adsorption by a maximum of 28.3 per cent and an average of 8 per cent.

CHAPTER VI

RECOMMENDATIONS

1. It is recommended that further work be done to obtain a more accurate method for delivering a specific amount of gas through the powder. One possibility for this method is some type of piston and cylinder arrangement.

2. Further investigation should be done using Knudsen-flow permeametry and mercury penetration porosimetry on porous materials having structural characteristics which differ from those tested to determine if the combined area from these two methods is equal to the gas adsorption area for materials in general.

APPENDIX

APPENDIX A

NOMENCLATURE

A	Cross-sectional area of bed, cm^2
K_1	A constant in the permeability equation for viscous flow
K_2	A constant in the permeability equation for Knudsen flow
L	Length of bed, cm
M	Molecular weight of gas, gram/mole
p	Gas pressure upstream of micrometer valve, mm Hg
$\bar{p}$	Mean pressure within the bed, mm Hg
Q	Gas flow rate, mole/cm^2-second
q	Gas volume, cm^3
R	Gas constant
S_w	Specific surface area of powder, m^2/gram
T	Absolute temperature, ^oK
t	Temperature, ^oC
W	Sample weight, grams
ΔP	Pressure loss across powder bed, dyne/cm^2
Δp	Pressure loss across powder bed, mm Hg
Δp_c	Corrected Pressure loss across powder bed, mm Hg
ϵ	Bed porosity
θ	Contact angle, degrees
ρ	Absolute powder density, gram/cm^3
ρ_B	Bulk powder density, gram/cm^3

η Gas viscosity, gram/cm-second

σ Surface tension, dyne/cm

τ Time required for q cm^3 of gas to flow, seconds

APPENDIX B

EXPERIMENTAL AND CALCULATED DATA

Permeametry Data and Results

Figure 10, a plot of Log Δp versus Log τ , is used to determine the resistance to flow due to the filter paper and support at a given flow rate.

Table 3 lists experimental and calculated permeametry data for all samples tested. Figures 11 and 12 are plots of Log S_w versus Δp for non-porous and porous samples, respectively, and are used to determine the true external surface area at zero pressure.

Porosimetry Data and Results

Porosimetry data for all samples tested is shown in Figures 13 through 21, plots of Penetration Volume versus Log Pore Diameter. Each of these curves is used to determine the internal pore area of the sample, and these results are tabulated in Tables 4 and 5.

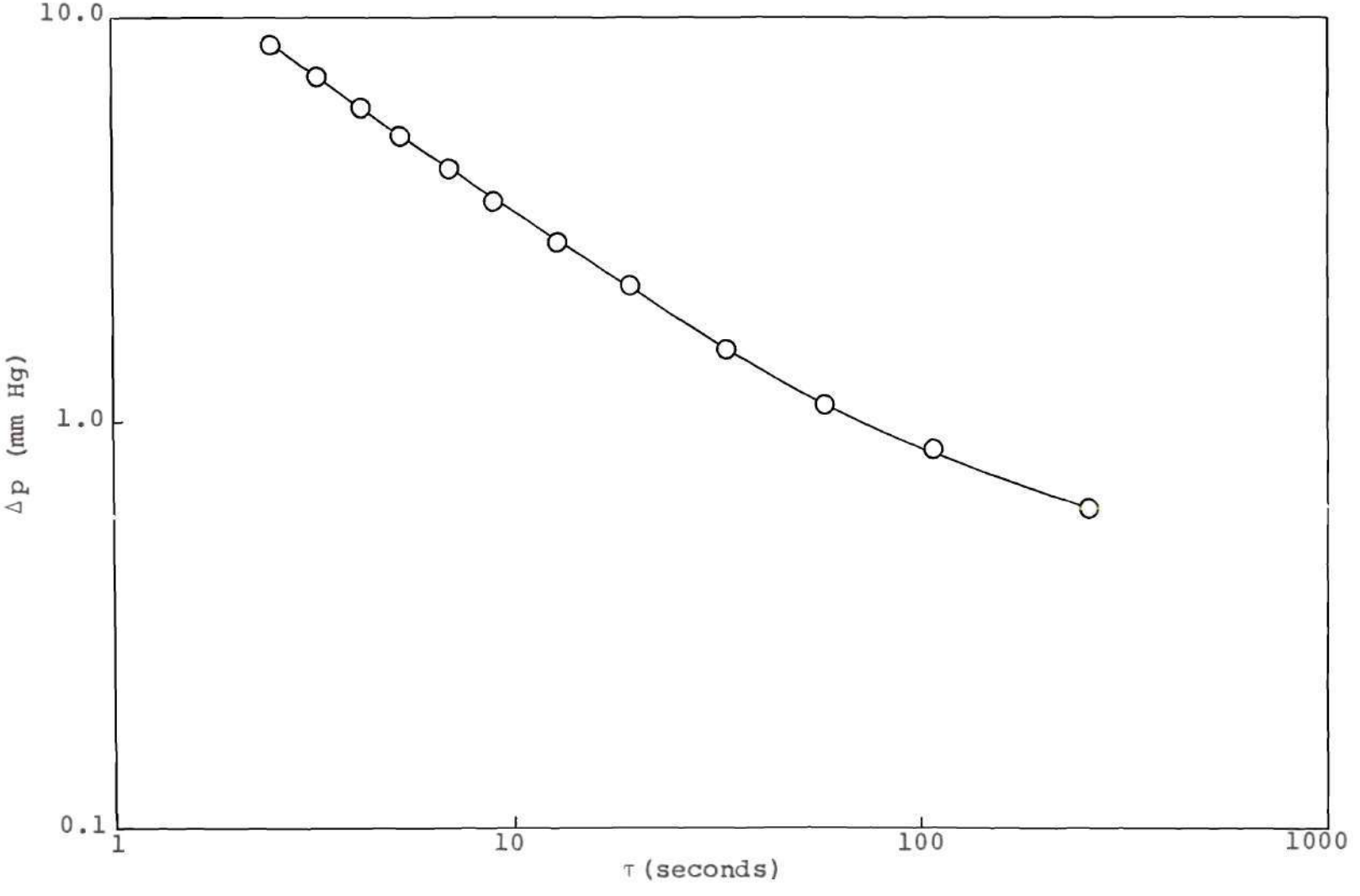

Figure 10. LogΔp versus Log τ .

Table 3. Measured and Calculated Permeameter Data

Measured Pressure Loss (mm Hg)	Time for Flow of 1 cc at 1000 mm Hg (seconds)	Corrected Pressure Loss (mm Hg)	Calculated Surface Area (m^2/g)
Iron blue; density, 1.70 gm/cc; sample weight, 0.2476 gm; bed length, 0.304 cm; ambient temperature, 24°C; porosity, 0.663.			
14.70	123.05	13.89	70.6
10.85	172.11	10.15	72.2
6.20	312.20	5.63	73.3
		Extrapolation	74.1
Titanium dioxide; density, 4.17 gm/cc; sample weight, 0.2698 gm; bed length, 0.216 cm; ambient temperature, 24°C; porosity, 0.789.			
15.45	66.50	14.41	51.5
9.80	109.80	8.98	53.0
6.08	190.10	5.42	55.1
		Extrapolation	57.0
Carbon black-A; density, 1.87 gm/cc; sample weight, 0.3955 gm; bed length, 0.312 cm; ambient temperature, 24°C; porosity, 0.522.			
13.60	59.10	12.51	11.9
9.12	92.20	8.22	12.2
6.49	138.50	5.74	12.7
4.40	225.20	3.78	13.6
		Extrapolation	14.0
Carbon black-B; density, 1.89 gm/cc; sample weight, 0.4541 gm; bed length, 0.328 cm; ambient temperature, 24°C; porosity, 0.485.			
14.68	40.50	13.30	6.51
9.10	72.00	8.10	7.02
5.92	118.22	5.11	7.29
3.30	240.05	2.68	7.80
		Extrapolation	8.0

Tungsten; density, 19.3 gm/cc; sample weight, 2.5891 gm; bed length, 0.272 cm; ambient temperature, 23.3°C; porosity, 0.653.

15.11	9.50	12.65	0.460
12.10	12.05	10.01	0.462
8.24	18.21	6.68	0.466
4.93	31.56	3.86	0.468
2.85	58.78	2.15	0.484
		Extrapolation	0.48

Polyvinyl chloride-A; density, 1.52 gm/cc; sample weight, 0.7410 gm; bed length, 0.730 cm; ambient temperature, 24°C; porosity, 0.529.

14.10	2.36	5.30	0.110
10.90	3.24	3.90	0.113
7.80	4.98	2.60	0.114
4.50	10.20	1.28	0.116
2.90	18.85	0.76	0.126
		Extrapolation	0.13

Polyvinyl chloride-B; density, 1.60 gm/cc; sample weight, 0.9061 gm; bed length, 1.114 cm; ambient temperature, 24°C; porosity, 0.643.

12.57	2.79	4.62	0.133
8.65	4.52	3.02	0.142
6.05	7.25	1.98	0.148
3.80	13.45	1.15	0.159
		Extrapolation	0.17

Polyvinyl chloride-C; density, 1.57 gm/cc; sample weight, 0.9263 gm; bed length, 1.132 cm; ambient temperature, 24°C; porosity, 0.633.

13.51	2.67	5.39	0.144
10.54	3.70	4.09	0.152
6.94	6.38	2.52	0.164
3.32	17.10	1.05	0.180
		Extrapolation	0.19

Polyvinyl chloride-D; density, 1.52 gm/cc; sample weight, 0.2825 gm; bed length, 0.382 cm; ambient temperature, 24°C; porosity, 0.659.

13.10	2.10	3.50	0.263
10.50	2.78	2.69	0.270
6.55	5.24	1.45	0.275
		Extrapolation	0.30

Cupric carbonate-A; density, 3.95 gm/cc; sample weight, 0.6869 gm; bed length, 0.354 cm; ambient temperature, 24°C; porosity, 0.654.

14.40	20.70	12.39	3.72
5.40	62.50	4.33	3.94
3.25	116.91	2.44	4.12
		Extrapolation	4.15

Cupric carbonate-B; density, 3.95 gm/cc; sample weight, 0.8148 gm; bed length, 0.392 cm; ambient temperature, 24°C; porosity, 0.631.

16.10	21.05	14.09	3.37
11.60	30.00	10.01	3.41
7.25	50.51	6.05	3.49
4.35	90.13	3.46	3.55
		Extrapolation	3.60

Boron nitride-A; density, 2.25 gm/cc; sample weight, 0.4357 gm; bed length, 0.306 cm; ambient temperature, 24°C; porosity, 0.555.

13.52	68.71	12.50	14.18
10.25	93.90	9.36	14.51
6.55	161.95	5.85	15.61
3.62	324.45	3.07	16.42
		Extrapolation	17.2

Boron nitride-B; density, 2.25 gm/cc; sample weight, 0.7424 gm; bed length, 0.396 cm; ambient temperature, 24°C; porosity, 0.413.

11.70	5.19	6.59	0.183
9.15	7.20	5.07	0.196
6.59	11.29	3.59	0.217
4.69	17.80	2.48	0.236
		Extrapolation	0.27

Iron oxide-A; density, 5.25 gm/cc; sample weight, 1.3387 gm; bed length, 0.446 cm; ambient temperature, 24°C; porosity, 0.597.

12.18	14.20	9.58	0.84
8.99	21.29	6.99	0.89
5.87	40.70	4.50	1.14
3.78	73.25	2.79	1.27
		Extrapolation	1.50

Iron oxide-B; density, 5.25 gm/cc; sample weight, 1.1871 gm; bed length, 0.348 cm; ambient temperature, 24°C; porosity, 0.543.

12.18	21.05	10.16	1.24
9.82	28.09	8.14	1.33
6.65	46.20	5.41	1.45
4.30	77.10	3.34	1.49
		Extrapolation	1.77

Iron oxide-C; density, 5.25 gm/cc; sample weight, 1.3389 gm; bed length, 0.376 cm; ambient temperature, 24°C; porosity, 0.505.

13.90	30.03	12.30	1.59
9.95	46.10	8.70	1.71
6.42	79.32	5.47	1.86
4.40	125.71	3.60	1.94
		Extrapolation	2.10

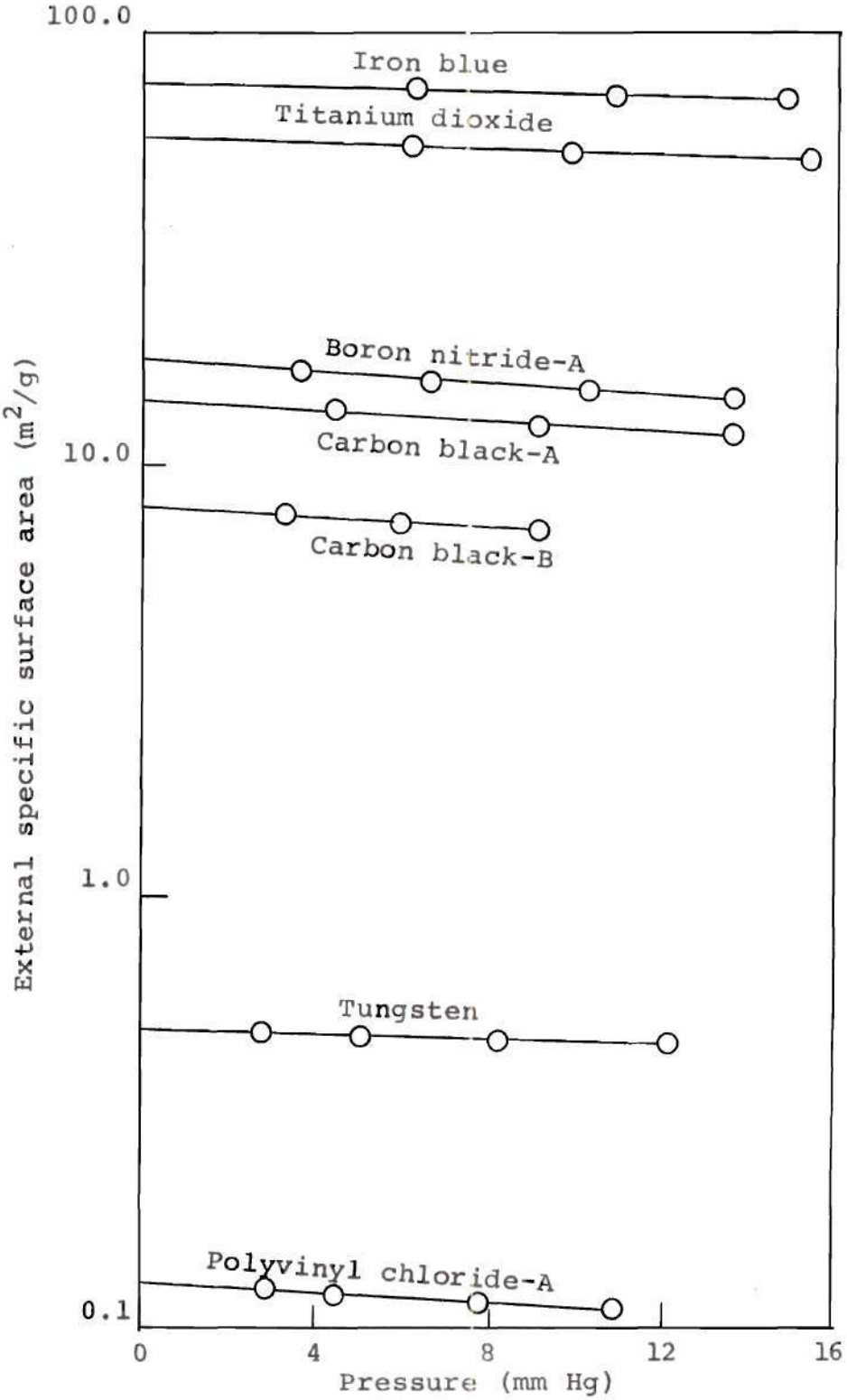

Figure 11. Specific Surface Area versus Pressure for Non-porous Samples.

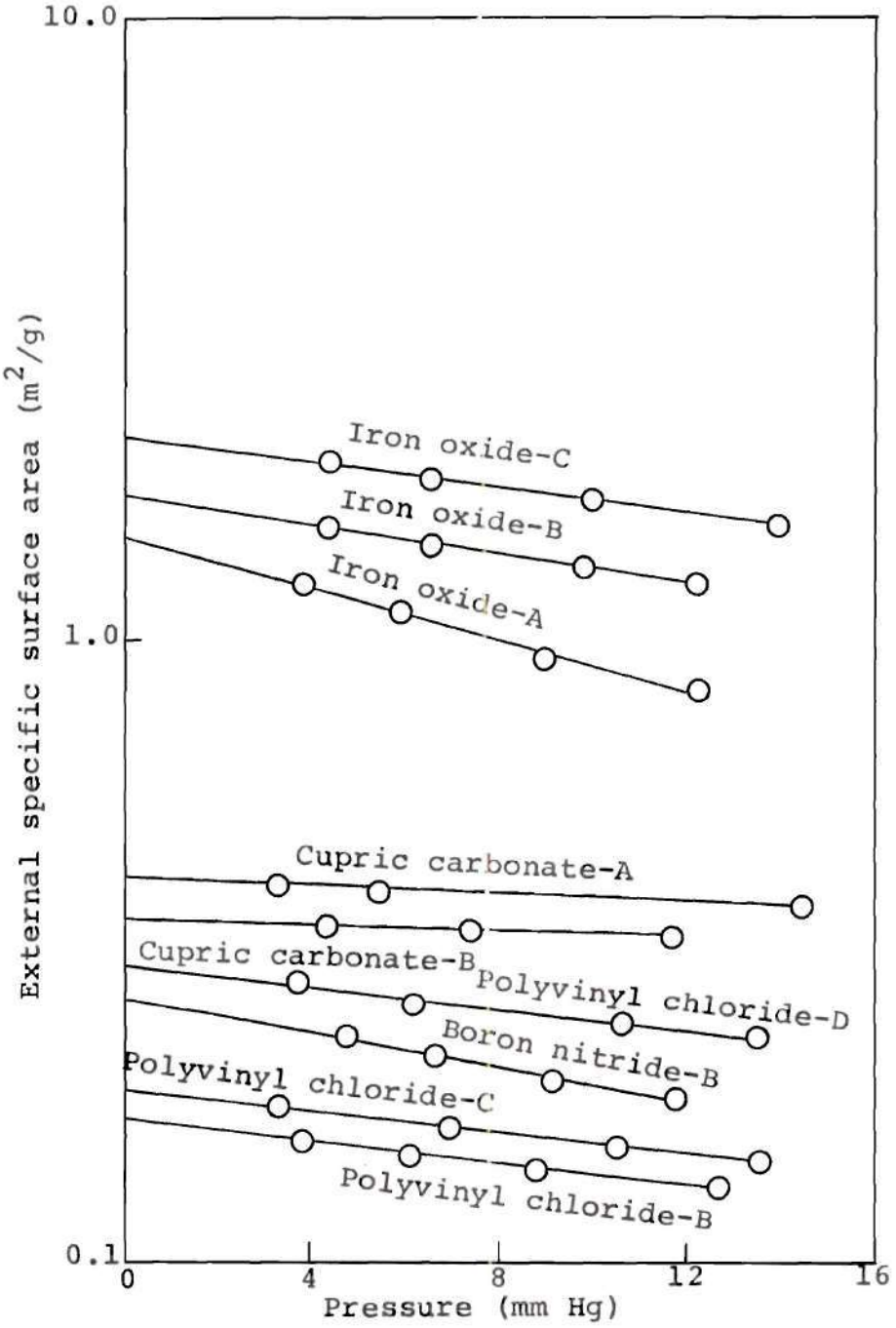

Figure 12. Specific Surface Area versus Pressure for Porous Samples.

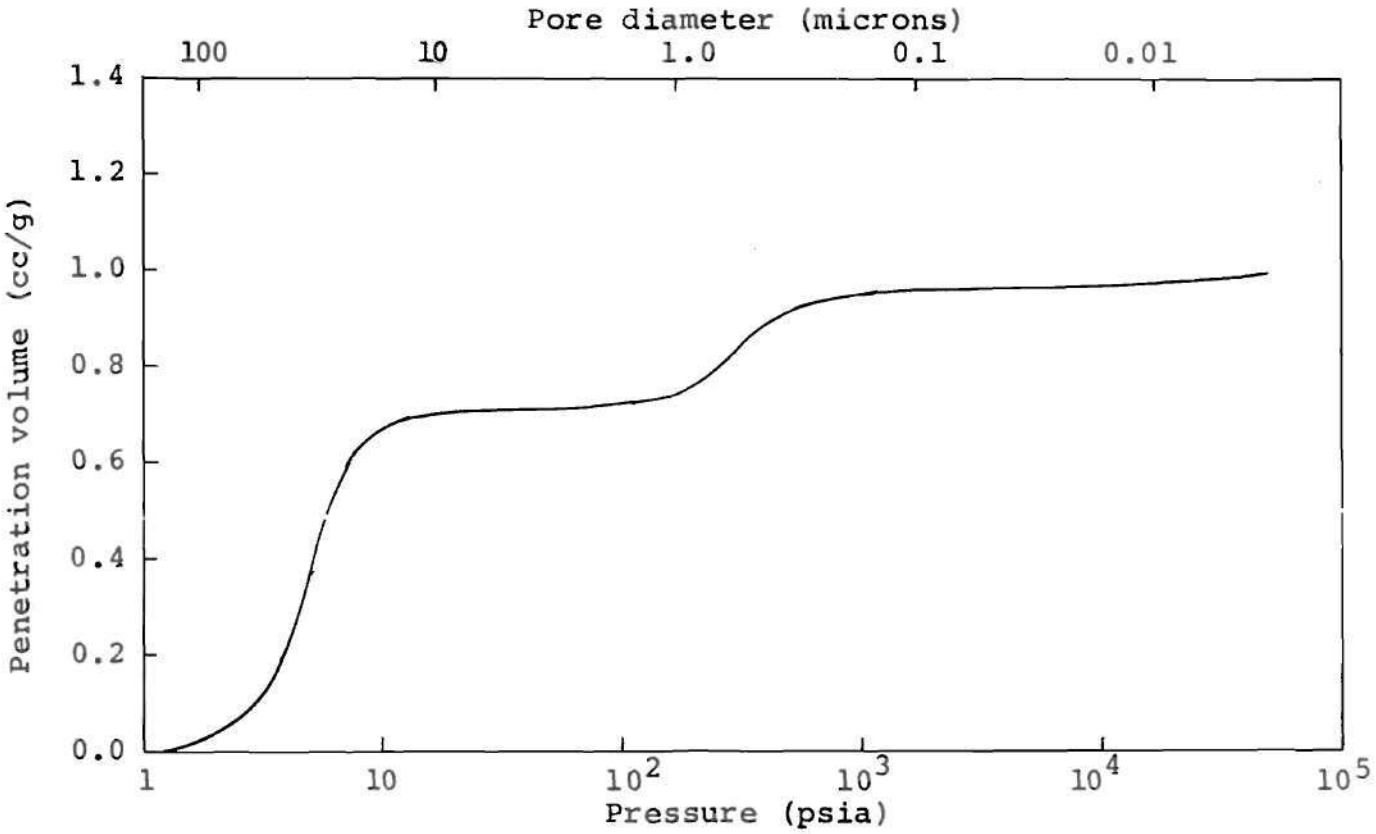

Figure 13. Penetration Volume versus Pore Diameter for Polyvinyl Chloride-B.

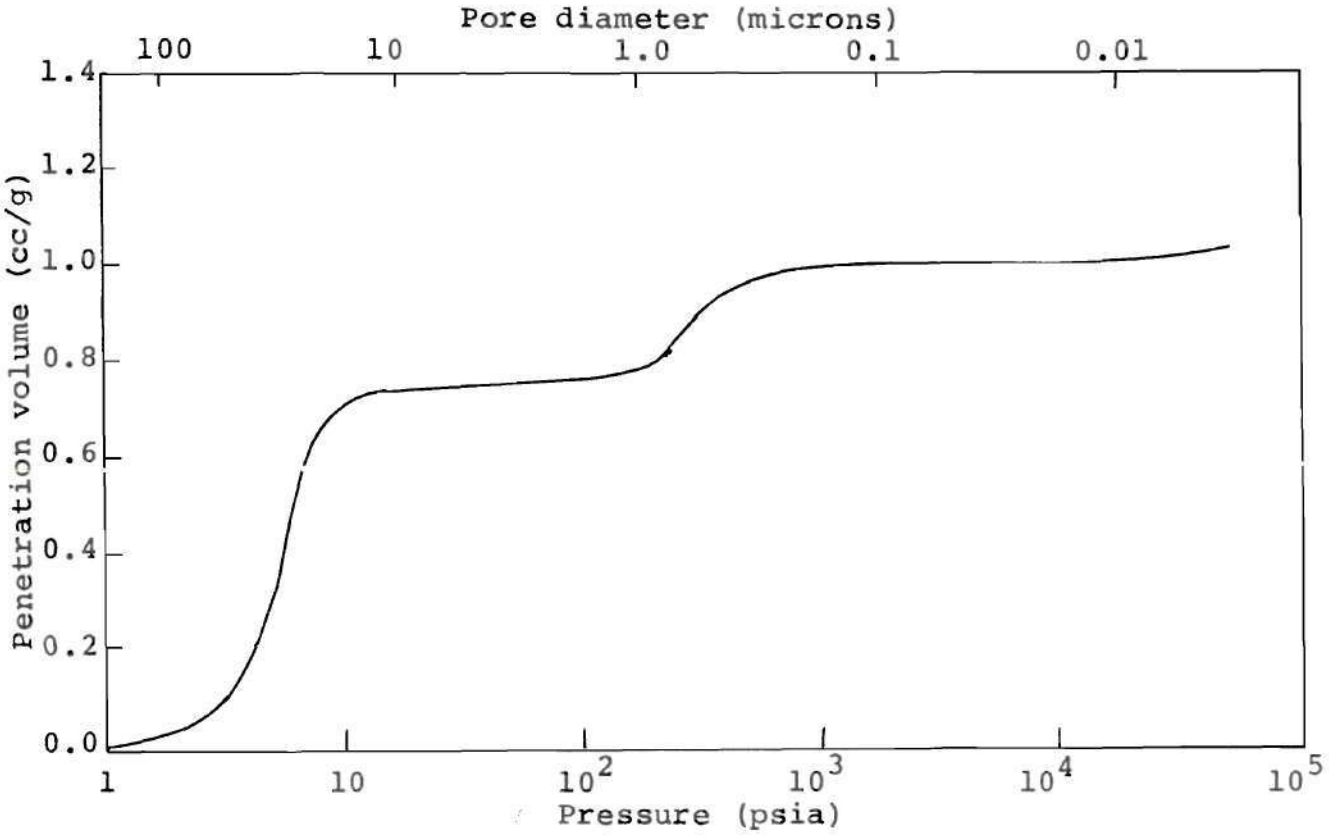

Figure 14. Penetration Volume versus Pore Diameter for Polyvinyl Chloride-C.

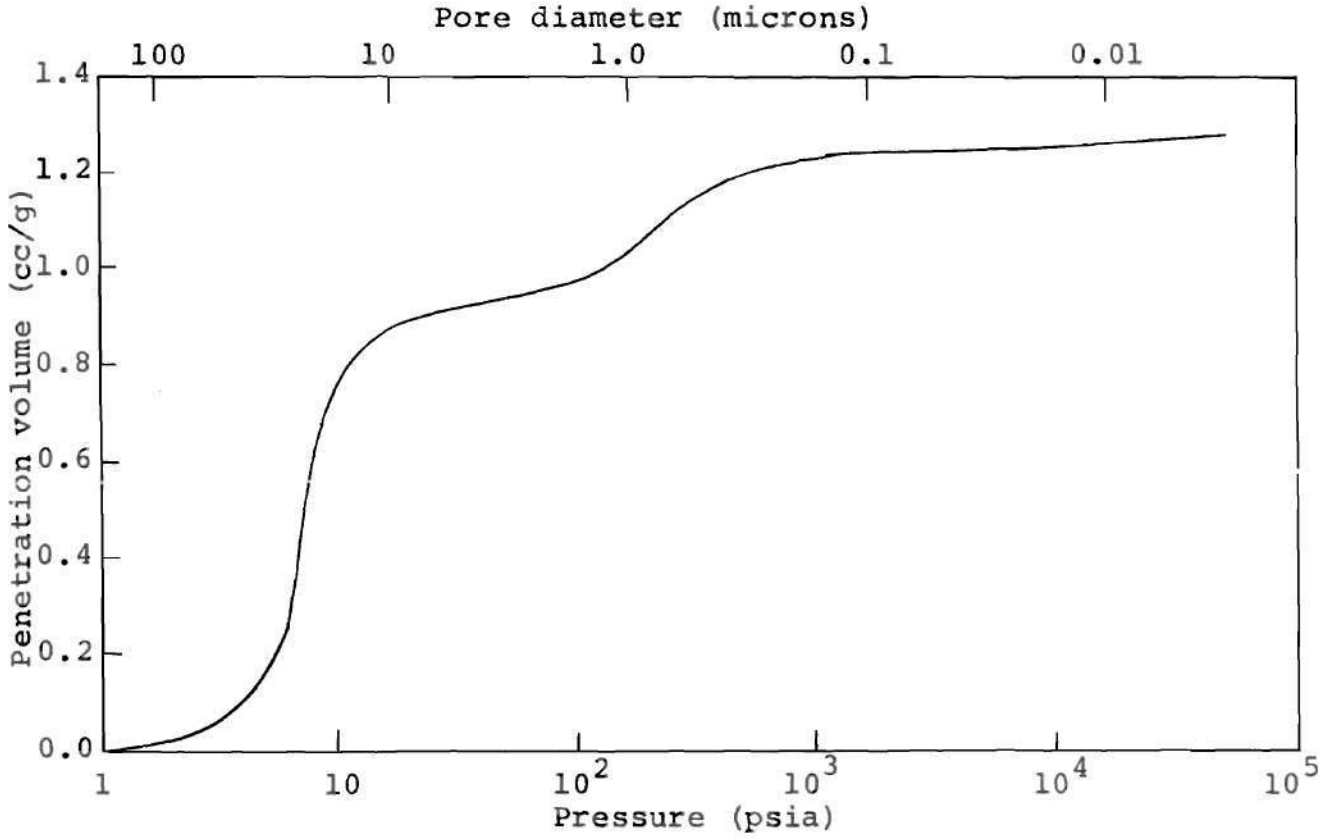

Figure 15. Penetration Volume versus Pore Diameter for Polyvinyl Chloride-D.

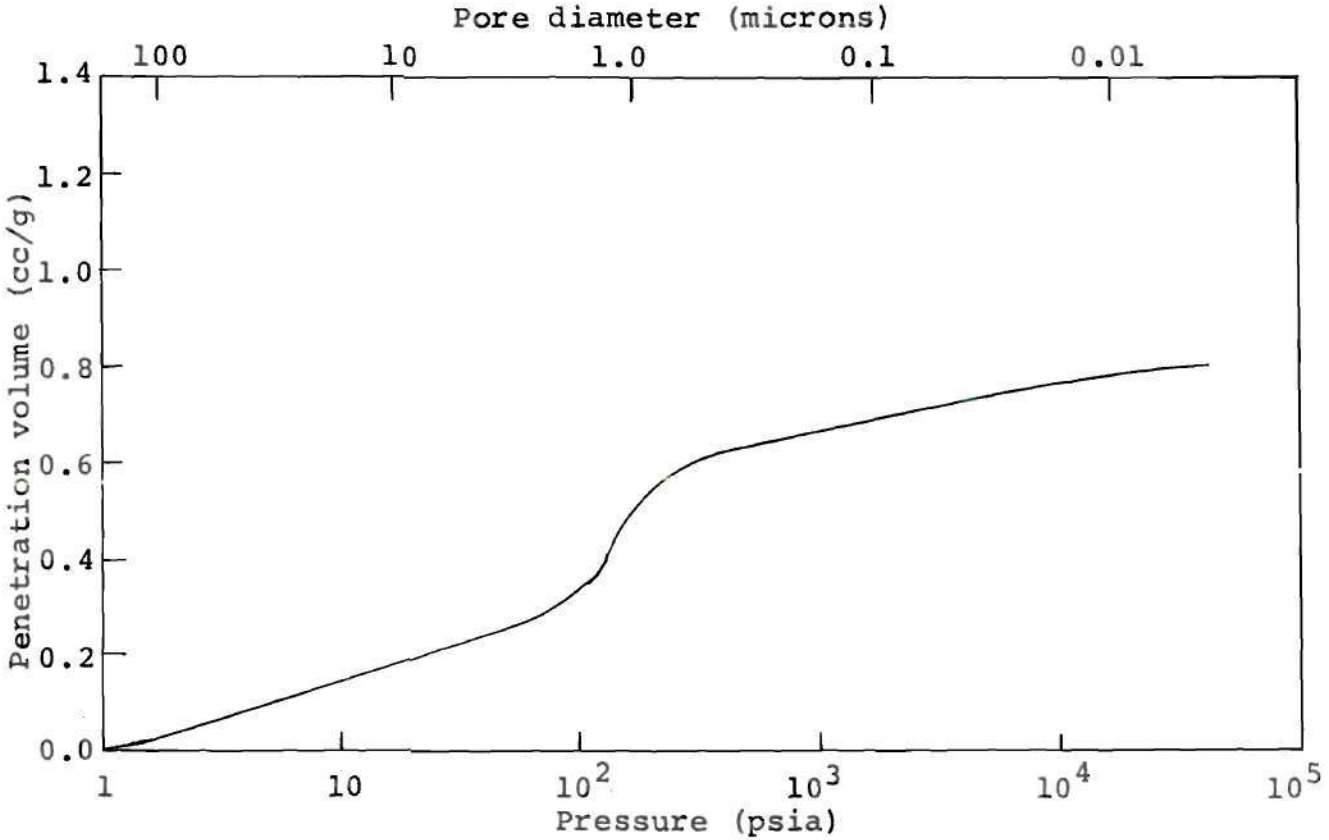

Figure 16. Penetration Volume versus Pore Diameter for Cupric Carbonate-A.

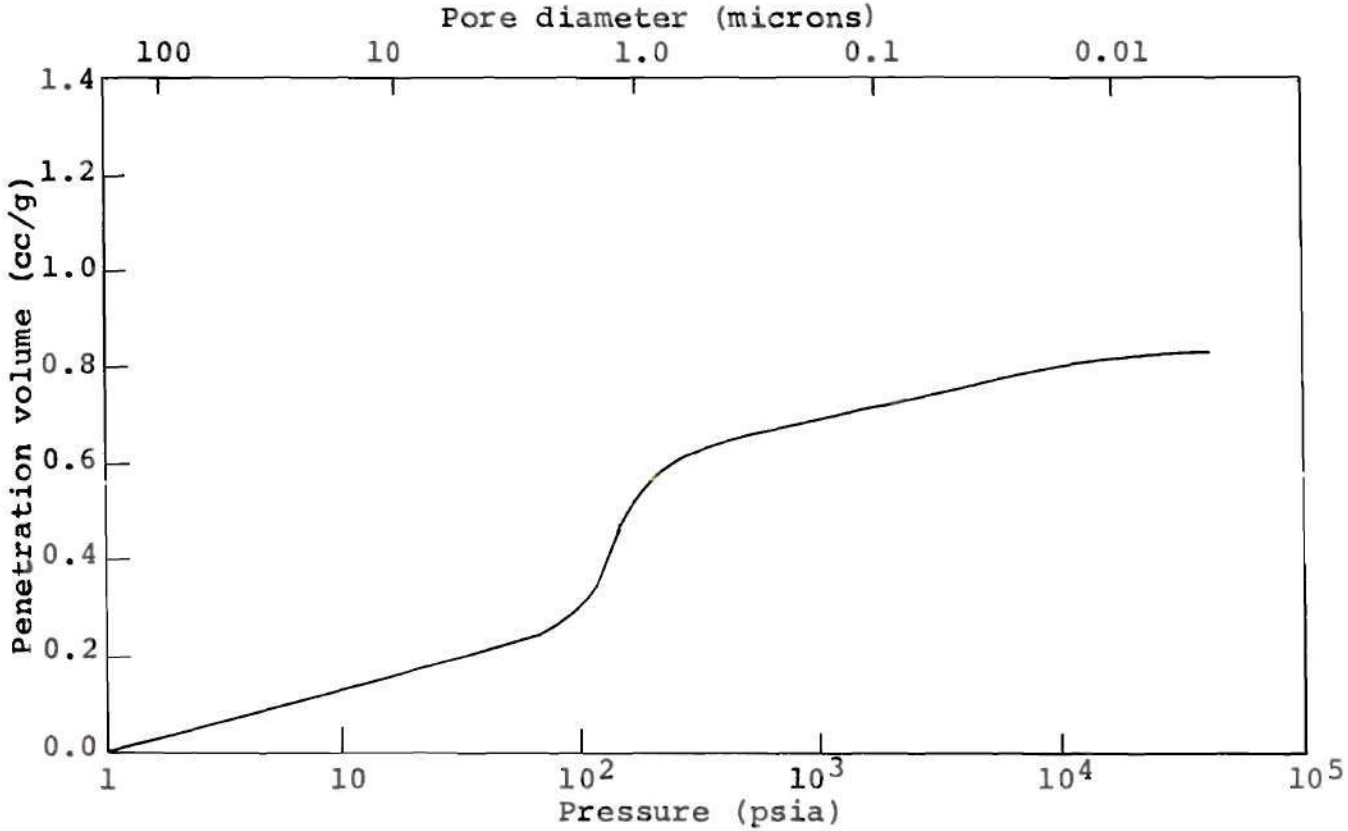

Figure 17. Penetration Volume versus Pore Diameter for Cupric Carbonate-B.

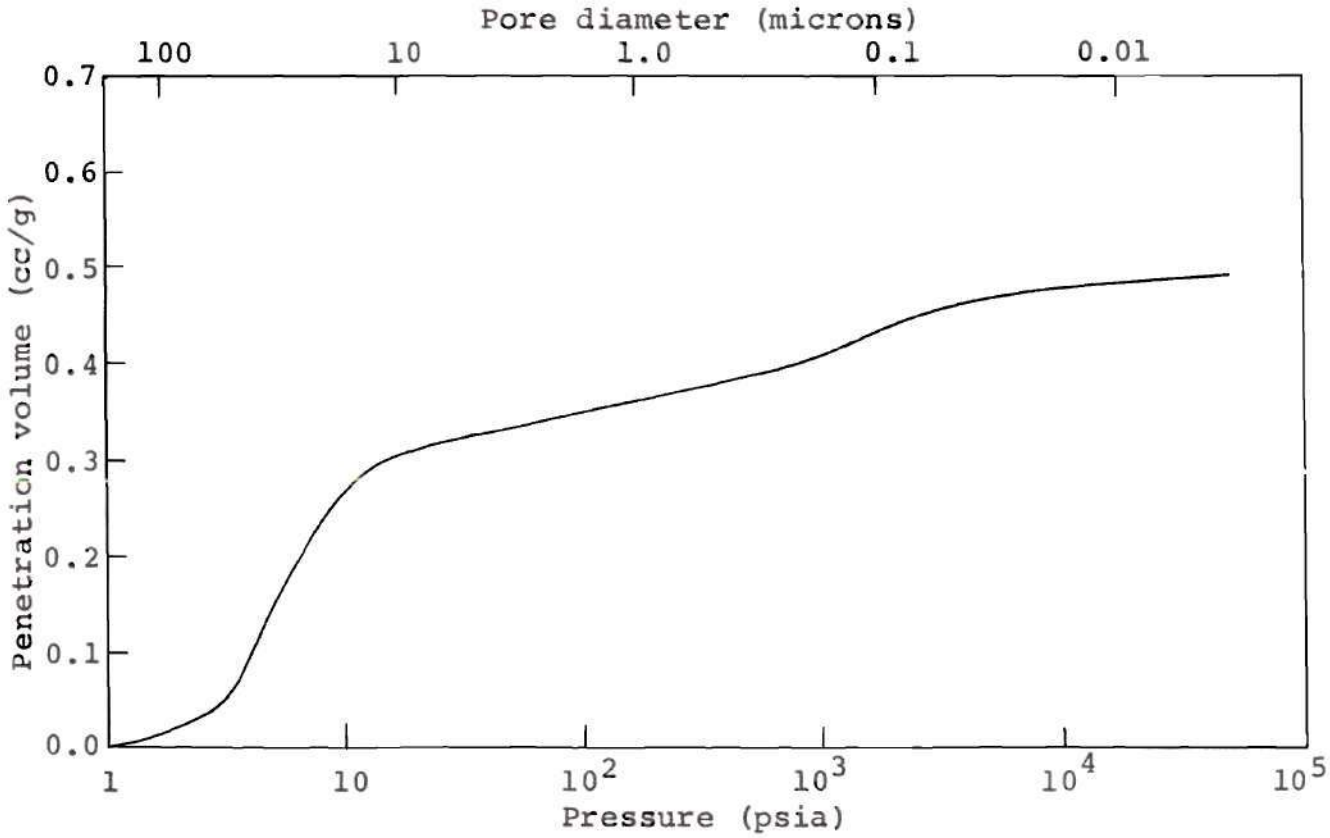

Figure 18. Penetration Volume versus Pore Diameter for Boron Nitride-B.

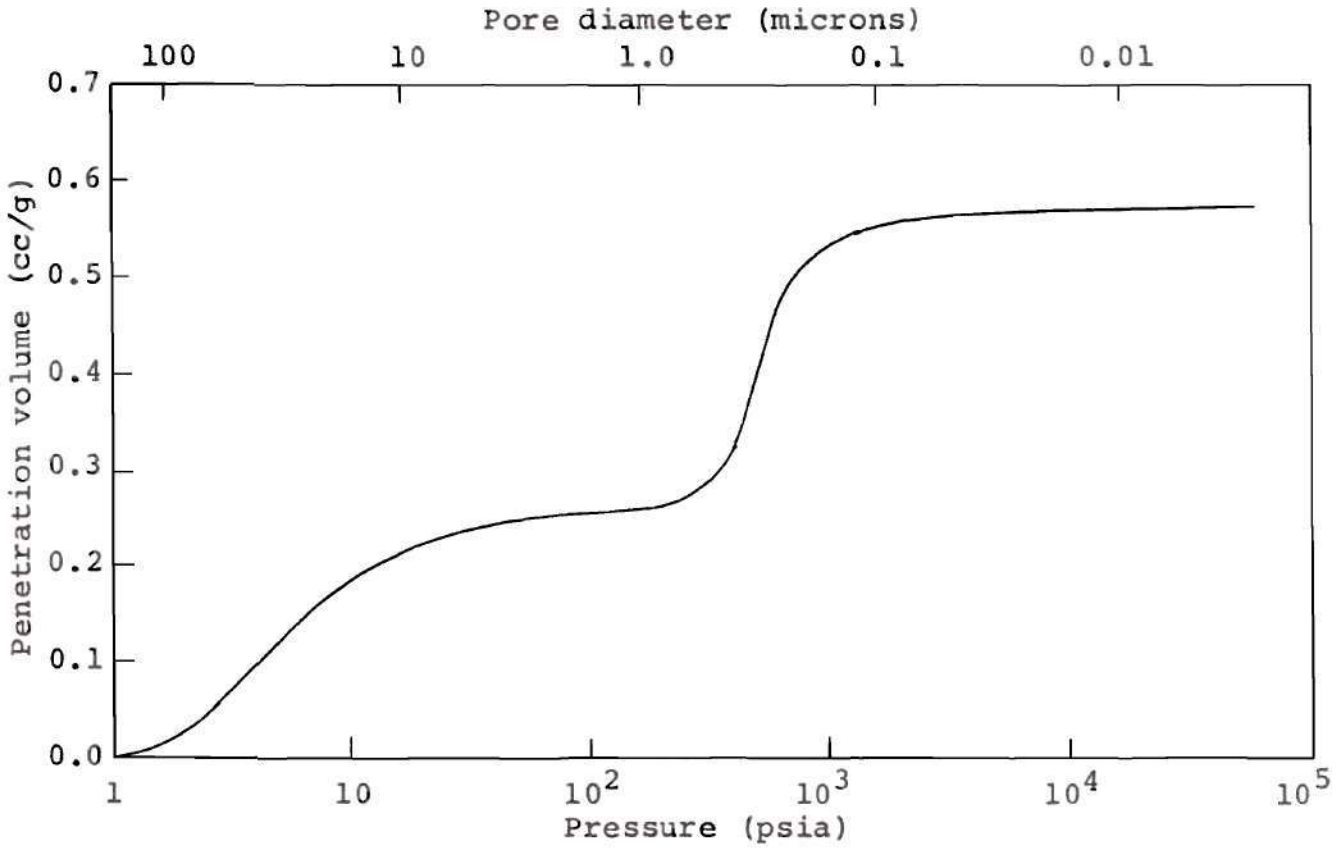

Figure 19. Penetration Volume versus Pore Diameter for Iron Oxide-A.

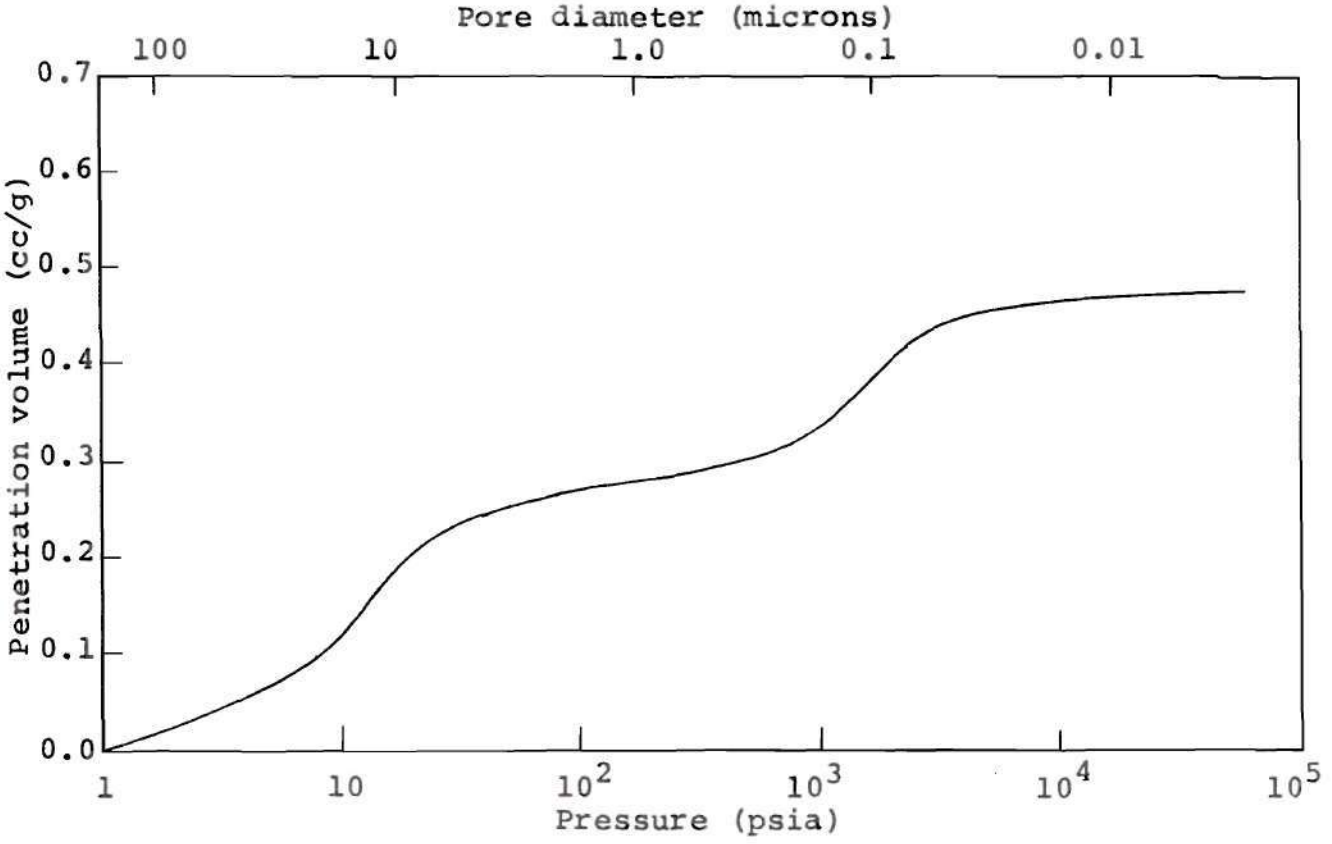

Figure 20. Penetration Volume versus Pore Diameter for Iron Oxide-B.

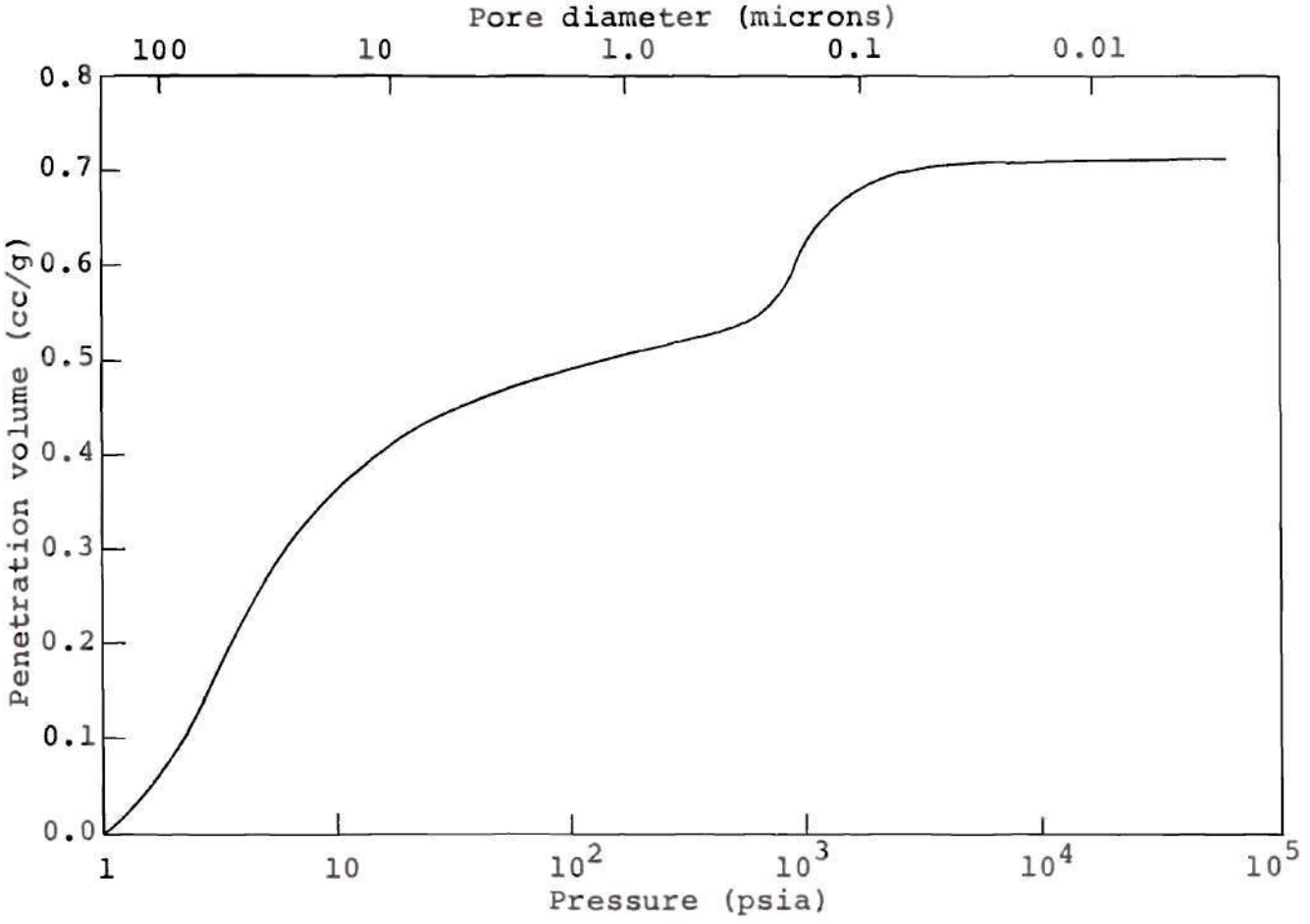

Figure 21. Penetration Volume versus Pore Diameter for Iron Oxide-C.

Table 4. Calculated Porosimeter Data
Using Graphical Integration

Polyvinyl Chloride-B		Polyvinyl Chloride-C	
Pressure Range (psia)	P·ΔV	Pressure Range (psia)	P·ΔV
80- 195	0.52	110- 170	0.04
195- 240	1.05	170- 243	1.65
240- 300	2.13	243- 300	2.02
300- 360	1.68	300- 360	1.70
360- 440	1.31	360- 450	1.91
440- 600	0.97	450- 750	2.98
600- 900	0.36	750- 1,600	0.66
900- 1,800	0.19	1,600- 5,100	0.28
1,800- 5,200	0.29	5,100-10,000	0.55
5,200-12,000	0.73	10,000-15,000	1.04
12,000-20,000	3.18	15,000-20,000	1.46
20,000-26,000	7.75	20,000-26,000	3.40
26,000-32,000	9.74	26,000-34,000	3.57
32,000-38,000	3.89	34,000-42,000	18.00
38,000-44,000	4.67	42,000-50,000	10.62
44,000-50,000	3.35		49.88
	41.81		

Area = 0.0225 x 41.81
= 0.94 m^2/g.

Area = 0.0225 x 49.88
= 1.12 m^2/g.

Polyvinyl Chloride-D

Pressure Range (psia)	P·ΔV
45- 79	0.09
79- 110	0.16
110- 160	1.35
160- 210	1.24
210- 280	1.61
280- 350	1.05
350- 440	0.79
440- 605	0.83
605- 960	0.44
960- 1,800	0.58
1,800- 3,600	0.38
3,600-10,000	1.06
10,000-20,000	3.43
20,000-26,000	1.32
26,000-32,000	4.88
32,000-40,000	7.10
40,000-50,000	6.96
	33.18

Area = 0.0225 x 33.18
= 0.75 m^2/g.

Cupric Carbonate-A

Pressure Range (psia)	P·ΔV
346- 416	5.33
416- 460	1.31
460- 507	2.90
507- 592	4.94
592- 684	2.55
684- 770	2.91
770- 885	4.96
885- 1,500	33.40
1,500- 1,950	15.52
1,950- 2,300	17.00
2,300- 2,800	20.40
2,800- 3,400	31.00
3,400- 4,200	34.22
4,200- 5,000	27.60
5,000- 6,300	62.10
6,300- 7,100	60.30
7,100- 8,000	60.40
8,000- 9,000	34.00
9,000-10,200	76.80
10,200-11,100	31.95
11,100-12,000	23.10
12,000-13,000	25.00
13,000-14,000	27.00
14,000-15,000	29.00
15,000-16,000	31.00
16,000-17,000	16.50
17,000-19,000	36.00
19,000-21,000	20.00
21,000-23,000	22.00
23,000-25,000	24.00
25,000-27,000	26.00
27,000-30,000	28.50
30,000-34,000	32.00
34,000-38,000	36.00
38,000-42,000	40.00
42,000-46,000	44.00
	989.69

Area = 0.0225 x 989.69
= 22.25 m^2/g.

Cupric Carbonate-B

Pressure Range (psia)	P·ΔV
565- 606	1.17
606- 650	3.14
650- 700	2.03
700- 765	1.46
765- 845	3.22
845- 905	7.87
905- 1,500	26.48
1,500- 2,000	15.75
2,000- 2,600	23.00
2,600- 3,150	25.87
3,150 3,600	30.40
3,600 4,200	31.20
4,200- 4,800	36.00
4,800- 5,500	41.20
5,500- 6,100	34.80
6,100- 6,800	38.70
6,800- 7,800	58.40
7,800- 9,000	42.00
9,000-10,000	28,50
10,000-11,000	21.00
11,000-12,000	23.00
12,000-13,000	25.00
13,000-15,000	28.00
15,000-17,000	16.00
17,000-20,000	18.50
20,000-32,000	26.00
32,000-40,000	36.00
40,000-50,000	44.00
	688.69

Area = 0.0225×688.69
= 15.48 $m^2/g.$

Boron Nitride-B

Pressure Range (psia)	P·ΔV
45- 49	0.02
49- 55	0.24
55- 75	0.35
75- 85	0.20
85- 96	0.21
96- 110	0.06
110- 125	0.31
125- 140	0.26
140- 150	0.29
150- 165	0.47
165- 180	0.17
180- 189	0.35
189- 240	1.29
240- 260	0.63
260- 290	0.82
290- 315	0.57
315- 360	0.32
360- 405	1.03
405- 460	0.87
460- 500	0.96
500- 590	2.18
590- 700	3.22
700- 800	2.25
800- 900	3.40
900-1,000	14.25
1,000-1,400	9.60
1,400-1,750	12.60
1,750-2,000	11.25
2,000-2,500	22.80
2,500-2,800	13.25
2,800-3,200	18.00
3,200-3,650	24.00
3,650-4,100	19.38
4,100-4,600	17.40
4,600-5,000	4.80
5,000-5,500	5.25
5,500-6,600	12.10
	201.94

Area = 0.0225×201.94
= 4.55 $m^2/g.$

Iron Oxide-A

Pressure Range (psia)	P·ΔV
90- 390	8.16
390- 760	119.00
760-1,900	70.40
1,900-4,000	1.77
	199.33

Area = 0.0225_2 x 199.33
= 4.48 m^2/g.

Iron Oxide-B

Pressure Range (psia)	P·ΔV
60- 75	0.31
75- 100	0.53
100- 150	0.76
150- 200	0.87
200- 350	2.78
350- 450	1.76
450- 600	4.10
600- 700	2.93
700- 800	4.58
800- 900	6.46
900- 1,100	15.30
1,100- 2,200	129.60
2,200- 3,400	79.60
3,400- 6,200	69.60
6,200- 8,000	14.90
8,000-10,000	1.80
10,000-14,000	20.41
	356.30

Area = 0.0225 x 356.30
= 8.02 m^2/g.

Iron Oxide-C

Pressure Range (psia)	P·ΔV
600- 700	23.60
700- 800	16.34
800- 900	17.68
900- 1,100	22.60
1,100- 2,200	88.10
2,200- 3,400	32.50
3,400- 6,200	8.16
6,200- 8,000	8.52
8,000-10,000	1.80
10,000-14,000	8.40
	227.70

Area = 0.0225 x 227.70
= 5.11 m^2/g.

Table 5. Calculated Porosimeter Data
Assuming Cylindrical Pores

Polyvinyl Chloride-B		Polyvinyl Chloride-C	
Pore Diameter Range (microns)	Surface Area Contribution (m^2/g)	Pore Diameter Range (microns)	Surface Area Contribution (m^2/g)
0.907 -2.21	0.017	1.040 -1.607	0.001
0.737 -0.907	0.026	0.728 -1.040	0.044
0.589 -0.737	0.054	0.589 -0.728	0.051
0.491 -0.589	0.041	0.491 -0.589	0.042
0.402 -0.491	0.033	0.383 -0.491	0.049
0.295 -0.402	0.024	0.236 -0.393	0.084
0.196 -0.295	0.010	0.111 -0.236	0.020
0.0982 -0.196	0.006	0.0347 -0.111	0.010
0.0340 -0.0982	0.010	0.0177 -0.0347	0.016
0.0144 -0.0340	0.022	0.0118 -0.0177	0.028
0.00884-0.0144	0.090	0.00884-0.0118	0.038
0.00680-0.00884	0.199	0.00680-0.00884	0.087
0.00553-0.00680	0.244	0.00520-0.00680	0.092
0.00466-0.00553	0.096	0.00421-0.00520	0.430
0.00402-0.00466	0.111	0.00354-0.00421	0.261
0.00354-0.00402	0.081		1.253
	1.054		

Polyvinyl Chloride-D

Pore Diameter Range (microns)	Surface Area Contribution (m^2/g)
2.24 -3.93	0.003
1.61 -2.24	0.004
1.11 -1.61	0.36
0.842 -1.11	0.032
0.631 -0.842	0.042
0.505 -0.631	0.026
0.402 -0.505	0.020
0.292 -0.402	0.022
0.184 -0.292	0.012
0.0982 -0.184	0.002
0.0491 -0.0982	0.001
0.0177 -0.0491	0.035
0.00884-0.0177	0.103
0.00680-0.00884	0.034
0.00553-0.00680	0.121
0.00442-0.00553	0.178
0.00354-0.00442	0.174
	0.845

Cupric Carbonate-A

Pore Diameter Range (microns)	Surface Area Contribution (m^2/g)
0.424 -0.511	0.120
0.384 -0.424	0.029
0.348 -0.384	0.066
0.299 -0.348	0.111
0.259 -0.299	0.057
0.229 -0.259	0.066
0.199 -0.229	0.112
0.117 -0.199	0.710
0.0904 -0.117	0.347
0.0766 -0.0904	0.384
0.0629 -0.0766	0.459
0.0518 -0.0629	0.699
0.0419 -0.0518	0.770
0.0352 -0.0419	0.623
0.0279 -0.0352	1.398
0.0248 -0.0279	1.369
0.0196 -0.0220	0.774
0.0173 -0.0196	1.739
0.0159 -0.0173	0.725
0.0147 -0.0159	0.524
0.0135 -0.0147	0.567
0.0126 -0.0135	0.614
0.0117 -0.0126	0.659
0.0110 -0.0118	0.705
0.0104 -0.0110	0.375
0.00927-0.0104	0.769
0.00839-0.00927	0.453
0.00769-0.00839	0.498
0.00707-0.00769	0.543
0.00655-0.00707	0.587
0.00589-0.00655	0.644
0.00520-0.00589	0.722
0.00465-0.00520	0.813
0.00421-0.00465	0.903
0.00385-0.00421	0.992
	22.195

Cupric Carbonate-B	
Pore Diameter Range (microns)	Surface Area Contribution (m^2/g)
0.292 -0.313	0.026
0.272 -0.292	0.071
0.253 -0.272	0.046
0.231 -0.253	0.033
0.209 -0.231	0.073
0.955 -0.209	0.178
0.118 -0.195	0.561
0.0884 -0.118	0.349
0.0680 -0.0884	0.511
0.0561 -0.0680	0.579
0.0491 -0.0561	0.684
0.0421 -0.0491	0.703
0.0368 -0.0421	0.812
0.0322 -0.0368	0.928
0.0290 -0.0322	0.734
0.0256 -0.0290	0.873
0.0227 -0.0260	1.317
0.0196 -0.0227	0.945
0.0177 -0.0196	0.643
0.0160 -0.0177	0.475
0.0147 -0.0161	0.520
0.0136 -0.0147	0.565
0.0118 -0.0136	0.630
0.0103 -0.0118	0.362
0.00884-0.0103	0.419
0.00552-0.00884	0.558
0.00441-0.00552	0.801
0.00369-0.00441	0.989
	15.135

Boron Nitride-B	
Pore Diameter Range (microns)	Surface Area Contribution (m^2/g)
2.08 -2.36	0.005
1.84 -2.08	0.005
1.61 -1.84	0.002
1.41 -1.61	0.007
1.26 -1.41	0.006
1.18 -1.26	0.007
1.07 -1.18	0.011
0.982 -1.07	0.004
0.936 -0.982	0.008
0.737 -0.936	0.029
0.679 -0.737	0.014
0.609 -0.679	0.019
0.561 -0.609	0.014
0.491 -0.561	0.030
0.436 -0.491	0.023
0.384 -0.436	0.019
0.353 -0.384	0.021
0.299 -0.353	0.049
0.253 -0.299	0.073
0.221 -0.253	0.051
0.197 -0.221	0.077
0.177 -0.197	0.321
0.126 -0.177	0.212
0.101 -0.126	0.283
0.0884-0.101	0.255
0.0706-0.0884	0.503
0.0631-0.0706	0.300
0.0553-0.0631	0.406
0.0484-0.0553	0.542
0.0431-0.0484	0.438
0.0384-0.0431	0.392
0.0354-0.0384	0.108
0.0321-0.0354	0.119
0.0267-0.0321	0.272
	4.605

Iron Oxide-A

Pore Diameter Range (microns)	Surface Area Contribution (m^2/g)
0.453 -1.964	0.110
0.233 -0.453	2.440
0.0931-0.233	1.321
0.0442-0.0931	0.349
	4,220

Iron Oxide-B

Pore Diameter Range (microns)	Surface Area Contribution (m^2/g)
2.357-2.947	0.006
1.768-2.357	0.011
1.179-1.768	0.016
0.884-1.179	0.019
0.505-0.884	0.058
0.393-0.505	0.039
0.295-0.393	0.090
0.253-0.295	0.064
0.221-0.253	0.102
0.196-0.221	0.145
0.161-0.196	0.344
0.080-0.161	2.700
0.052-0.080	1.720
0.028-0.052	1.451
0.022-0.028	0.336
0.018-0.022	0.040
0.013-0.018	0.425
	7.566

Iron Oxide-C

Pore Diameter Range (microns)	Surface Area Contribution (m^2/g)
0.253-0.295	0.529
0.221-0.253	0.367
0.197-0.221	0.398
0.161-0.197	0.508
0.080-0.161	1.835
0.052-0.080	0.704
0.029-0.052	0.170
0.022-0.029	0.192
0.018-0.022	0.040
0.013-0.018	0.017
	4.760

APPENDIX C

SAMPLE CALCULATIONS

Calculation of External Surface Area by Permeametry

Equation 4 is the starting point for external specific surface area calculations:

$$S_w = \frac{24}{13}\sqrt{\frac{2}{\pi}}\ \frac{\epsilon^2 A\ \Delta P}{(1-\epsilon)\rho L Q (MRT)^{\frac{1}{2}}} \qquad (4)$$

This equation may be rearranged to give:

$$S_w = 0.481\ \frac{\epsilon^2 A\ \tau}{\rho_B q (M(273 + t))^{\frac{1}{2}} L}\ \Delta p \left[\frac{760}{p} \times \frac{(273 + t)}{273}\right] \qquad (5)$$

In the system employed, A = 1.42 cm^2, M = 4 gram/mole, p = 1000 mm Hg, and q = 1.0 cm^3. Also, the correct value of Δp, called Δp_c, is obtained by subtracting a value read from Figure 10 from the measured Δp. Therefore, Equation 5 may be rewritten as:

$$S_w = 0.000952\ \frac{\epsilon^2 (273 + t)^{\frac{1}{2}} \Delta p_c\ \tau}{\rho_B\ L} \qquad (6)$$

As a sample calculation, the data for iron blue will be used to calculate a value for specific surface area:

$$\rho = 1.70 \text{ gram/cm}^3$$
$$W = 0.2476 \text{ gram}$$
$$L = 0.304 \text{ cm}$$
$$t = 24^{\circ}C$$

$$\epsilon = 1 - \frac{W}{AL} = 1 - \frac{0.2476}{(1.42)(0.304)(1.70)} = 0.663$$

$$\rho_B = \frac{W}{AL} = \frac{0.2476}{(1.42)(0.304)} = 0.573$$

$$S_w = \frac{0.000952(0.663)^2(273 + 24)^{\frac{1}{2}}\Delta p_c{}^{\tau}}{(0.573)(0.304)} = 0.0414\Delta p_c{}^{\tau}$$

At a measured pressure loss of 14.70 mm Hg, the time required for 1 cubic centimeter of helium to flow through the bed was 123.05 seconds. From Figure 10, it can be observed that the resistance due to the filter paper and support at this flow rate is equal to 0.81 mm Hg. Therefore:

$$\Delta p_c = 14.70 - 0.81 = 13.89 \text{ mm Hg}$$
$$S_w = 0.0414(13.89)(123.05) = 70.6 \text{ m}^2/\text{gram}$$

Values of S_w are calculated as above at the two other pressure loss values, and these values of S_w are plotted against pressure loss on semi-logarithmic paper in Figure 11. The true value of external specific surface area is obtained by extrapolating the straight line to zero pressure. In this example:

$$S_w = 74.0 \text{ m}^2/\text{gram}$$

Calculation of Internal Surface Area by Porosimetry

The internal surface areas of the powders investigated were determined using mercury penetration porosimetry. The data from the porosimeter were used directly to plot curves of penetration volume versus applied pressure (Figures 13-21). From these curves, the internal surface areas of the powders were calculated using two different techniques.

The first technique (21) was developed by assuming that the work dW required to immerse an area dA of a non-wetting material in mercury was:

$$dW = \sigma(\cos\theta)dA \tag{7}$$

This work was supplied when the applied pressure P forced a volume of mercury dV into the pores. Equation 7 became:

$$\sigma(\cos\theta)dA = -PV \tag{8}$$

or

$$A = \frac{-\int PdV}{\sigma(\cos\theta)} \tag{9}$$

Since the surface tension of mercury was 474 dyne/cm and the contact angle was assumed to be 130°, Equation 9 became:

$$A = 0.0225 \int PdV \tag{10}$$

The total internal area was obtained by graphically integrating the curve of penetration volume versus pressure and multiplying the result by 0.0225. It should be noted that this technique of calculating pore area involved no assumption of a particular pore geometry. Therefore, the areas obtained using this method were taken to be the true internal areas of the powders.

The calculation of the internal surface area of iron oxide-A using the above technique is presented as an example.

Pressure Range (psia)	Mean Pressure (psia)	Increment of Volume (cc/g)	$P \cdot \Delta V$
90- 390	240	0.034	8.16
390- 760	575	0.207	119.00
760-1900	1330	0.053	70.40
1900-4000	2950	0.006	1.77
			199.33

$$\text{Internal Area} = 0.0225 \times 199.33$$
$$= 4.48 \text{ m}^2/\text{g}.$$

The second technique for calculating internal area required the assumption that all pores were right circular cylinders. The pore area was equal to πdh and the pore volume was equal to $\pi r^2 h$. Combining these expressions gave:

$$\text{Pore Area} = \frac{4 \times \text{Volume}}{\text{Diameter}} \qquad (11)$$

Diameter values were determined using the expression given

in the porosimeter manual:

$$\text{Diameter} = \frac{176.8}{\text{Applied Pressure}} \qquad (12)$$

The total internal area was obtained by dividing the curve of penetration volume versus pore diameter into a number of increments; determining the mean diameter and the penetration volume change of each increment; calculating the internal area contribution per increment using Equation 11; and summing these internal area contributions.

The calculation of the internal surface area of iron oxide-A using the second technique is presented.

Sample weight = 1.4220 grams

Cell Factor = 0.000774 cc/count

Applied Pressure (psia)	Corrected Counter Indication	Pore Diameter (microns)	Volume of Pores of Indicated Diameter and Larger (cc/g)	Per Cent of Pores Having Volumes Greater Than Indicated Diameter
90	485	1.964	0.264	0.0
390	548	0.453	0.298	11.4
760	930	0.233	0.506	80.4
1900	1027	0.093	0.559	98.0
4000	1038	0.044	0.565	100.0

From the above values, the following values are calculated:

Diameter Range (microns)	Pore Mean Diameter (microns)	Volume of Pores in Diameter Range (cc/g)	Area of Pores in Diameter Range (m^2/g)
0.453-1.964	1.208	0.034	0.11
0.233-0.453	0.343	0.207	2.44
0.093-0.233	0.263	0.053	1.32
0.044-0.093	0.068	0.006	0.35
			4.22

The internal areas for the nine porous powders calculated using the two above techniques are shown in Table 6. It is evident that the areas compare favorably.

Table 6. Comparison of Internal Areas from Two Techniques

Material	Internal Area using Graphical Integration (m^2/g)	Internal Area Assuming Cylindrical Pores (m^2/g)
Cupric carbonate-A	22.25	22.20
Cupric carbonate-B	15.48	15.14
Boron nitride-B	4.55	4.60
Iron oxide-A	4.48	4.22
Iron oxide-B	8.02	7.57
Iron oxide-C	5.11	4.76
Polyvinyl chloride-B	0.94	1.05
Polyvinyl chloride-C	1.12	1.25
Polyvinyl chloride-D	0.75	0.85

BIBLIOGRAPHY

(1) P. C. Carman, Flow of Gases Through Porous Media, Academic Press, New York, 1956, 81-103.

(2) R. D. Cadle, Particle Size, Reinhold, New York, 1965, 132-134.

(3) Clyde Orr, Jr., "Specific Surface Area by Low Pressure Permeametry," Analytical Chemistry, 39, 1967, 834-836.

(4) B. H. Kaye, "Permeability Techniques for Characterizing Fine Powders," Powder Technology, 1, 1967, 11-22.

(5) Clyde Orr, Jr., and J. M. DallaValle, Fine Particle Measurement, MacMillan, New York, 1959, 134-163.

(6) Terrence Allen, Particle Size Measurement, Chapman and Hall, London, 1968, 171-189.

(7) P. C. Carman, "Fluid Flow Through Grannular Beds," Transactions of the Institution of Chemical Engineers, 1937, 15, 150-166.

(8) P. C. Carman, "The Determination of the Specific Surface of Powders. I," Transactions of the Institution of Chemical Engineers, 1938, 57, 225-234.

(9) F. M. Lea and R. W. Nurse, "The Specific Surface of Fine Powders," Journal of the Society of Chemical Industry, Transactions, 58, 1939, 277-283.

(10) P. J. Rigden, "The Specific Surface of Powders. A Modification of the Air-Permeability Method for Rapid Routine Testing," Journal of the Society of Chemical Industry, Transactions, 62, 1943, 1-4.

(11) P. J. Rigden, "The Specific Surface of Powders. A Modification of the Theory of the Air-Permeability Method," Journal of the Society of Chemical Industry, Transactions, 66,1947, 130-136.

(12) J. C. Arnell, "Permeability Studies. I. Surface Area Measurement using a Modified Kozeny Equation," Canadian Journal of Research, 24A, 1946, 103-116.

(13) R. M. Barrer and D. M. Grove, "Flow of Gases and Vapours in a Porous Medium and its Bearing on Adsorption Problems," Transactions of the Faraday Society, 47, 1951, 826-844.

(14) F. A. Schwertz, "The Structure of Porous Materials from Gas Penetration Rates," Journal of Applied Physics, 20, 1949, 1070-1075.

(15) G. Kraus, J. W. Ross and L. A. Girifalco, "Surface Area Analysis by Means of Gas Flow Methods, I. Steady State Flow in Porous Media," Journal of Physical Chemistry, 57, 1953, 330-333.

(16) L. B. Loeb, Kinetic Theory of Gases, Dover, New York, 1961, 280-291.

(17) W. G. Pollard and R. D. Present, "On Gaseous Self-Diffusion in Long Capillary Tubes," Physical Review, 73, 1948, 762-774.

(18) G. Kraus and J. W. Ross, "Surface Area Analysis by Means of Gas Flow Methods. II. Transient State Flow in Porous Media." Journal of Physical Chemistry, 57, 1953, 334-336.

(19) B. V. Deryagin, Akad. Nauk SSSR, 53, 1946, 623-626.

(20) Clyde Orr, Jr., "Application of Mercury Penetration to Materials Analysis," Powder Technology, 3, 1969/70, 117-123.

(21) H. M. Rootare and C. F. Prenzlow, "Surface Areas from Mercury Porosimeter Measurements," Journal of Physical Chemistry, 71, 1967, 2733-2736.